TITLE
ASP Conference Series, Vol. **VOLUME***, **YEAR OF PUBLICATION**
NAMES OF EDITORS

Spatial Correlations of Phase Relationships in TRACE Ultraviolet Bandpasses

Scott W. McIntosh

Universities Space Research Association, CPSS, Seabrook, MD 20706.

Laboratory for Astronomy and Solar Physics, NASA/GSFC, Mailcode 682.3, Greenbelt, MD 20771.

Bernhard Fleck

European Space Agency, Research and Scientific Support Department, NASA/GSFC, Mailcode 682.3, Greenbelt, MD 20771.

Abstract. We present the results of an investigation into the interaction of the topographic structure of the solar chromospheric plasma with the wave modes manifesting themselves in the UV continua formed there. We show that there is a distinct correlation between the inferred plasma topography and the phase-differences in different levels of the solar atmosphere. We interpret these factors as evidence of interaction between the oscillations and the extended magnetic "canopy".

1. Introduction

The question still exists as to the exact evolutionary path, from generation to extinction, of the ubiquitous oscillations observed in the quiet solar chromosphere. The underlying goal of this quest is to assess whether or not there is a sufficient wave flux to supply energy, through some as yet unidentified mechanism, to the ambient chromospheric and coronal plasmas. In recent simulations (Rosenthal et al. 2001; Bogdan et al. 2002, 2003) and observational investigations (Krijger et al. 2001, Judge, Tarbell & Wilhelm 2001; McIntosh et al. 2001; McIntosh & Judge 2001; McIntosh & Smillie 2003) the plasma's magnetic topology, or "canopy", has been demonstrated to have a significant influence on the chromospheric oscillations and, in particular, how and where (spatially and spectrally) they are observed.

As an extension of previous analyses (see, e.g., Lites, Chipman & White 1982; Deubner & Fleck 1990) we will construct and consider the spatial variation of phase-difference spectra between the 1550, 1600 & 1700 Å UV continuum bandpasses of the Transition Region and Coronal Explorer (TRACE; Handy et al. 1999). Previously, these quantities have been studied in a spatially unresolved (average) sense; looking at global network and inter-network regions and the qualitative differences between them. We will make a break from this norm and suggest that physically meaningful information exists in phase-difference and cross-power spectra on spatial scales down to a spatial resolution of $2.5''$, or some five TRACE pixels, by forming phase-difference (x,y) "maps". At this

reduced spatial resolution we can, in principle, interpret these maps in terms of the magnetic/thermodynamic structure and connectivity of the network and inter-network chromospheric plasma. In Sect. 2 we will demonstrate, by means of a specific example, our data analysis method, providing error estimates and demonstrating how those errors vary as a function of spatial resolution. In Sect. 3 we illustrate the correlation between the phase relationships and the extrapolated magnetic "canopy" that we derive from a (simple) potential field extrapolation of the co-aligned Solar and Heliospheric Observatory (SOHO; Fleck, Domingo & Poland 1995) Michelson Doppler Imager (MDI; Scherrer et al. 1995) line-of-sight high resolution magnetogram.

We see that a strong spatial correlation exists between the inferred plasma topography and the phase-difference maps derived from the TRACE UV continua. We briefly discuss the implications of this correlation for the symbiotic interaction of chromospheric oscillations and the chromospheric canopy. The interested reader is pointed to McIntosh, Fleck & Judge (2003) for further discussion of the results presented in this paper.

2. Data Analysis

As a specific example of our analysis method we will analyze the SOHO and TRACE Joint Observing Program 72 (JOP72) dataset of February 26, 1999 (23:00-24:00 UT) which was been discussed in detail by Judge, Tarbell & Wilhelm (2001) and later by McIntosh & Judge (2001). We use our sample hour-long (240 frames at a 15 second cadence) TRACE dataset to form a two-dimensional time-series dataset (x,y,t; i.e. a data-cube $D_\lambda(x, y, t)$). Since our objective is to compute Fourier Transforms of the time-series of each spatial pixel we must ensure that the image dataset is as stable as possible and alleviate the motion of features[1]. After performing an FFT at each spatial pixel to give $F_\lambda(x, y, \nu)$ of each cube we compute the cross-spectrum $C_{ij}(x, y, \nu)(= F_i \cdot F_j^\dagger$; where superscript † indicates the complex conjugate of the quantity) of the three bandpass pairs (1700-1600; 1700-1550; 1600-1550). The real and imaginary parts of the cross-spectrum provide the phase-difference ($tan(\Delta\phi_{ij}) = \Im C_{ij}/\Re C_{ij}$) and cross-power ($CP_{ij}(x, y, \nu) = |C_{ij}|^2$) between the bandpass pairs.

Lites, Chipman & White (1982) and Deubner & Fleck (1990) computed "phase-o-grams" (bivariate histograms of phase-difference versus frequency) from phase-difference spectra of ground-based observables to study the progression of phase as a function of frequency; Fig. 1(left) provides example phase-o-grams for the studied TRACE bandpass pairs. In each of the phase-o-grams we see the clear spine of the phase-difference behavior with frequency below ∼15 mHz where noise begins to dominate each timeseries signal. Note that the spine is clear in this case because the phase-o-grams are normalized to the maximum value at each frequency. To measure the spatial variation in the phase-difference

[1]This step is performed by an Interactive Data Language routine of the "Solarsoft" tree tr_get_disp_2d.pro which maps subsequent frames to those at t=0 by performing a Fourier transform based correlation between subsequent frames by minimizing the spatial deviation of the correlation maxima.

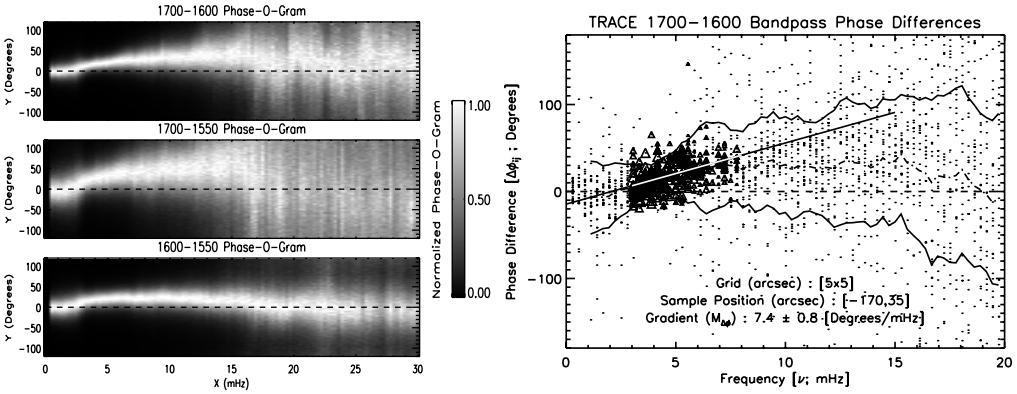

Figure 1. A normalized "phase-o-gram" for the entire inter-network region present in each of the TRACE UV bandpasses is shown in the left figure. Notice the phase-shift spine and its variation with frequency. At each frequency the distribution is normalized to its maximum value. In the right figure we show the phase-o-gram for one typical inter-network 5×5 super-pixel from which we derive the linear-fit determined phase-difference gradient, $M_{\Delta\phi}$.

we create phase-o-grams for a reduced resolution "super-pixel" element of say, 5×5 pixels (or $2.5''$), and perform a linear fit evaluating gradient $M_{\Delta\phi}$, from the resulting cross-power weighted spine over a fixed range of frequencies. In this case we choose the frequency range to be 3-8 mHz[2]. In the right hand plot of Fig. 1 we show an example of the $M_{\Delta\phi}$ fit in a typical inter-network 5×5 super-pixel between the 1700Å and 1600Å bandpasses. The scatter-plot shows the phase-difference frequency space (small dots) for each of the 25 full-resolution spatial pixels incorporated in each super-pixel of F_λ. Between 3 and 8 mHz we show triangles for the points used in the fit with their size proportional to the cross-power and relative weighting contribution to the linear fit. In this case there is a value of 7.4 ($\pm$ 0.8; least-squares error) Degrees mHz^{-1}.

Clearly, errors in the computation in $M_{\Delta\phi}$ vary with the size of the $N \times N$ super-pixel desired; the larger values of N refine the scatter of the phase-o-gram in the 3-8 mHz band but in doing so reduces the capability to form a spatial map of $M_{\Delta\phi}$ with a reasonable amount of feature contrast and so the choice is clearly a trade-off. By changing N and computing the resulting error in the fit (each computed with an additional 100 realizations of the fit with Monte-Carlo randomly adjusted fitting weights; $CP_{ij} \pm \sqrt{CP_{ij}}$) we see that, in the left-hand plot in Fig. 2, the values scale significantly with N.

As a test of our methodology we perform a "closure" calculation (cf. Sect. 2 of Krijger et al. 2001) by evaluating the difference between the 1700-1550 $M_{\Delta\phi}$ map and the sum of the 1700-1600 and 1600-1550 $M_{\Delta\phi}$ maps, again, for different

[2]We recognize that this frequency range encompasses evanescent waves near/below the acoustic cut-off frequency and propagating waves, this choice is critical when trying to asses what type of wave mode is present but not when trying to assess the degree of spatial variation, as is the case in this paper.

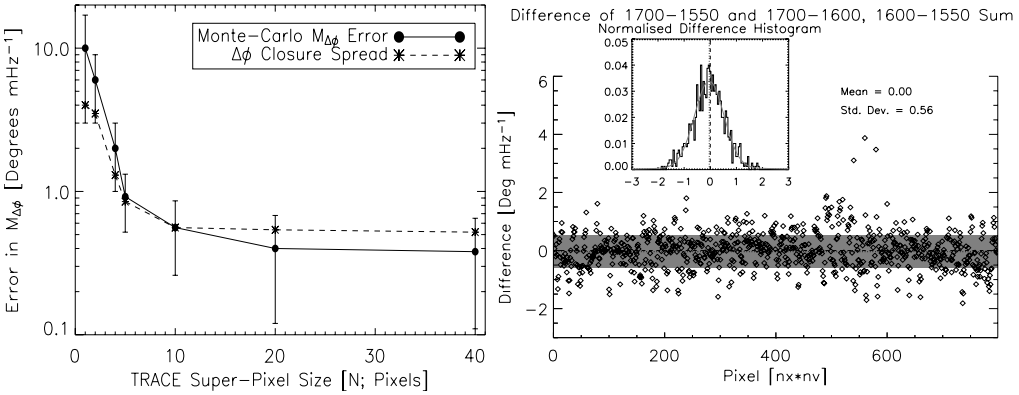

Figure 2. The scaling of the Monte-Carlo computed error in $M_{\Delta\phi}$ as a function of the TRACE super-pixel size, N. There is a steady decease in the error from full-spatial resolution going below 1 Degree mHz^{-1} at around $N = 5$. In the right-hand figure we show the closure calculation for $M_{\Delta\phi}$ we see that, for the $N = 10$ maps studied, there is a mean of zero with a small deviation (0.56), the grey shaded area is standard deviation about the mean. The spread of the phase closure is also related to N (see the dashed line in the left-hand figure).

values of N. Put quite simply the difference should be zero with some spread due to the use of $M_{\Delta\phi}$ as a parametric proxy of the full spatially unresolved phase-difference changes with frequency. In the right-hand side of Fig. 2 we show a closure test for the $N = 10$ case and see that there is a zero mean and spread of 0.56 Degrees mHz^{-1}. The variation of the closure spread with N is shown in the left-hand side of Fig. 2 and again we see a steady decrease as N increases.

3. Results

Using the technique outlined in the previous section we can form spatial maps of $M_{\Delta\phi}$ with a spatial resolution varying from full $0.5''\times0.5''$TRACE resolution elements out to $20''\times20''$resolution element super-pixels. However, the need to have a reasonable contrast between network and inter-network regions requires that we reduce our linear spatial resolution to say $2.5''$or $5.0''$which have acceptable errors ($\sim$1 Degree mHz^{-1}) and a small closure spread ($\sim$0.6 Degree mHz^{-1}). In panels B through D of Fig. 3 we show the spatial of $M_{\Delta\phi}$ in each of the three bandpass pairs. Clearly, there is considerable contrast between different inter-network regions as well as betwen those and the network-elements where the maps show very low values of $M_{\Delta\phi}$.

Since our stated objective was to show how the phase-difference correlates to the chromospheric plasma topography, or canopy, we need to construct a sample. To do this we perform a potential extrapolation of the time-averaged MDI $B_{||}$ in the TRACE field-of-view. Once the three dimensional field $B(x, y, z, t = 0)$ is calculated from $B_{||}$(x,y,z=0) we compute the magnetic pres-

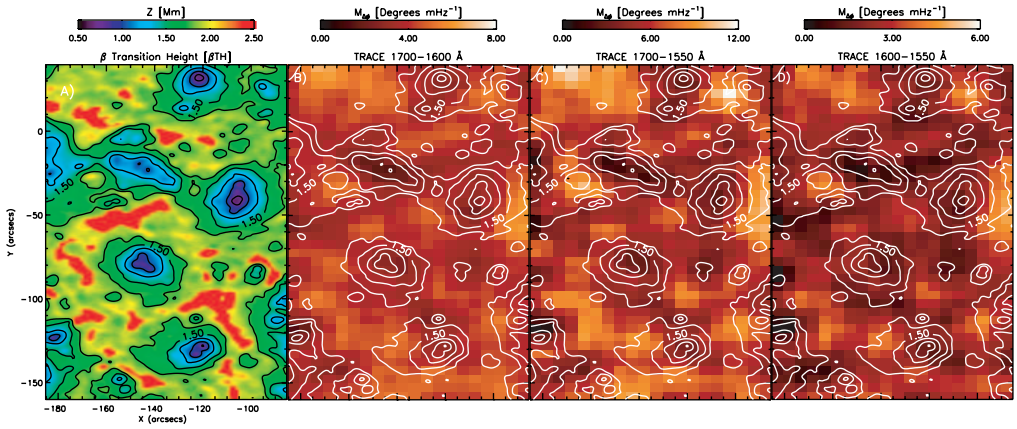

Figure 3. Panel A shows the model-derived altitudes at which the plasma-β is of order unity in the TRACE field of view (βTH) with $N = 5$ super-pixel resolution. In panels B through D we show the fitted phase-difference gradient ($M_{\Delta\phi}$) maps as discussed in the text. We note more than a passing correspondence between the overplotted contours (each separated by 0.25 Mm) and the darker regions of the $M_{\Delta\phi}$ maps.

sure $P_{\rm B}(x, y, z) = B_{||}(x, y, z)^2/8\pi$ and the plasma-β ($\beta \equiv P_{\rm g}/P_{\rm B}$; where $P_{\rm g}$ is the model gas pressure). We use the VAL3C (Vernazza, Avrett & Loeser 1981) model $P_{\rm g}$ values interpolated onto the same vertical scale as that of the magnetic field extrapolation. In panel A of Fig. 3 we show a map of the vertical height in each spatial pixel at which the plasma-β is of order unity; the plasma-β transition height or $\beta - TH$. By comparing panels B through D with panel A we see that the highest values of $M_{\Delta\phi}$ occur where the $\beta - TH$ is high. Correspondingly, as the canopy expands out of the network elements and into the inter-network plasma we often see progression from dark (low $M_{\Delta\phi}$) to lighter (higher $M_{\Delta\phi}$) regions.

Unfortunately, despite the clear and compelling correlation between the maps of topographic structure (through $\beta - TH$) and the phase-difference maps we have to remember that the phase-difference is not a "clean" diagnostic of the plasma topography. The phase-difference gradient, $M_{\Delta\phi}$, is proportional to the difference in the TRACE bandpass formation heights (Δz_{ij}) and the reciprocal of the phase-speed (V_{phase}) of any perturbation present there, $M_{\Delta\phi} \approx \Delta z_{ij}/V_{phase}$. Therefore, the results at this early stage must be interpreted with extreme care.

4. Future Considerations

For the time being, the investigation of these phase-difference/canopy interaction effects (as well as attempts to resolve the convolution of wave phase-speed and spectral formation layer) will be limited to the complex, though not impossible, combination of spectroscopic slit (SUMER) and passband imaging (TRACE) observations which lack Doppler velocity information (cf. Judge, Tarbell &

Wilhelm 2001). Indeed, that will be the case until we are able to perform some form of imaging spectroscopy. Such a platform will allow the study of multiple line profiles simultaneously, spanning the vertical domain of the solar atmosphere in a less discrete fashion. This advance will accurately allow the diagnosis and mapping of the important region where the plasma-β is of order unity.

Acknowledgments. SWM acknowledges the support of a External Fellowship from the European Space Agency at GSFC and the European Solar Magnetometry Network (ESMN) under contract ERBFMRXCT980190.

References

Bodgan, T. J., Rosenthal, C. S., Carlsson, M., et al. 2002, Astron. Nachr., 323, 196

Bodgan, T. J., Rosenthal, C. S., Carlsson, M., et al. 2003, In Press, ApJ

Deubner, F.-L. & Fleck, B. 1990, A&A, 228, 506

Fleck, B., Domingo, V. & Poland, A. I. 1995, The SOHO Mission, Dordrecht: Kluwer

Handy, B. N., Acton, L. W., Kankelborg, C. C., et al. 1999, Solar Phys., 187, 229

Judge, P. G., Tarbell, T. D. & Wilhelm, K. 2001, ApJ, 554, 424

Krijger, J. M., Rutten, R. J., Lites, B. W., et al. 2001, A&A, 379, 1052

Lites, B. W., Chipman, E. G. & White, O. R. 1982, ApJ, 253, 367

McIntosh, S. W., Bogdan, T. J., Cally, P. S., et al. 2001, ApJ, 548, L237

McIntosh, S. W. & Judge, P. G. 2001, ApJ, 561, 420

McIntosh, S. W., Fleck B., Judge, P. G. 2003, A&A, 405, 769

Rosenthal, C. S., Bogdan, T. J., Carlsson, M., et al. 2002, ApJ, 564, 508

Scherrer, P. H., Bogart, R. S., Bush, R. I., et al. 1995, Solar Phys., 162, 129

Title, A. M., Topka, K. P., Tarbell, T. D., et al. 1992, ApJ, 393, 782

Vernazza, J. E., Avrett, E. H. & Loeser, R. 1981, ApJS, 45, 635

Wilhelm, K., Curdt, W., Marsch, E., et al. 1995, Solar Phys., 162, 189